Utilization of Teak Wood Powder as a Carbon Source in LiFePO_4/C Cathode Lithium-Ion Batteries

Widiyandari, Hendri
Department of Physics, Faculty of Mathematics and Natural Sciences, Sebelas Maret University

Alfi Nur Aini
Department of Physics, Faculty of Mathematics and Natural Sciences, Sebelas Maret University

Rahmawati, Mintarsih
Centre of Excellence for Electrical Energy Storage Technology, Sebelas Maret University

Purwanto, Hery
Department of Physics, Faculty of Mathematics and Natural Sciences, Sebelas Maret University

https://doi.org/10.5109/7236875

出版情報：Evergreen. 11 (3), pp.2324-2331, 2024-09. 九州大学グリーンテクノロジー研究教育センター
バージョン：

Utilization of Teak Wood Powder as a Carbon Source in $LiFePO_4$/C Cathode Lithium-Ion Batteries

Hendri Widiyandari[1,2,*], Alfi Nur Aini[1], Mintarsih Rahmawati[2], Hery Purwanto[1]
[1]Department of Physics, Faculty of Mathematics and Natural Sciences, Sebelas Maret University, Indonesia
[2]Centre of Excellence for Electrical Energy Storage Technology, Sebelas Maret University, Indonesia

*Author to whom correspondence should be addressed:
E-mail: hendriwidiyandari@staff.uns.ac.id

(Received November 3, 2023; Revised September 2, 2024; Accepted September 7, 2024).

Abstract: $LiFePO_4$ has a weakness in the form of low conductivity (10^{-9} S/cm). One of the efforts to increase electrical conductivity is through carbon coating. This study used a carbon source from teak sawdust (*Tectona grandis*). Synthesis of carbon by carbonization method with temperature variations of 350, 450, and 550°C and through the activation process. The synthesis of LFP/C used the solid-state method due to the simplicity of the process. Based on the SEM-EDX results, the carbon morphology appears to be microfibrils with the highest carbon content of 81.73%. The results of XRD and FTIR analysis showed that the LFP/C cathode material had an orthorhombic structure. Meanwhile, the SEM results show the morphology of the material in the form of a polyhedral. EIS testing has been carried out with the highest conductivity value of 3.31 x 10^{-3} S/cm and the results of the specific capacity obtained the highest value of 36.18 mAh/g.

Keywords: Teak wood powder; Lithium-ion battery; Cathode; $LiFePO_4$; Conductivity

1. Introduction

The depletion of fossil fuels encourages the development of clean energy technologies and sustainable transportation options in order to reduce environmental problems such as acid rain, air pollution, and global warming. Innovating new alternative energy sources is encouraged by this[1)]. One of the necessities of human life is the battery, an electrical energy storage device. Generally, batteries can be divided into primary batteries for single use and secondary batteries that can be used repeatedly. Sodium ions, lithium ions, and nickel metal hydride (NiMH) batteries are among the secondary batteries whose development has accelerated recently. However, because of its high capacity and long cycle life, lithium-ion battery is the most used secondary battery[2,3)].

Anode, cathode, separator, and electrolyte are the four main parts of a lithium-ion battery[4)]. High capacity is produced by the cathode. Lithium cobalt oxide ($LiCoO_2$), was the first cathode material to be commercially successful. Its low level of safety as a result of the high cobalt content is its weakness[5)]. Other cathode components include lithium nickel cobalt oxide (NCA) materials have high capacity but low safety, lithium manganese oxide (LMO) materials have high thermal stability but a low capacity, lithium nickel manganese cobalt oxide (NMC) materials have high specific energy but low thermal stability[6)]. Lithium iron phosphate ($LiFePO_4$) is an excellent cathode material for use in electric vehicles due to its advantages such as high theoretical capacity (170 mAh/g)[7)], non-toxicity, long cycle life, high level of safety and cheap raw material prices. However, the weakness of $LiFePO_4$ is its low conductivity (10^{-9} S/cm). Efforts to increase electrical conductivity include ion doping, minimizing particle size, and carbon coating. Among these efforts, carbon coating is an effective approach that can increase the electrical conductivity of $LiFePO_4$[8)].

The presence of abundant natural resources that produce biomass waste, such as coconut shells, rice husks, corn cobs, and sawdust, helps in fulfilling the demand for activated carbon in Indonesia. Utilization of sawdust is usually used to meet the needs of industry as boiler fuel. One of the carbon content in natural materials is teak wood sawdust which can be processed into activated carbon[9,10)]. Numerous studies have been performed on the conversion of waste into carbon electrodes, with a focus on biomass waste[3)]. The carbon source for the $LiFePO_4$/C cathode material in this study was teak wood powder using the carbonization method which is anticipated to be a useful solution to environmental issues[11)].

Several synthesis methods in $LiFePO_4$/C include solid state, sol-gel, co-precipitation, hydrothermal, carbothermal reduction, and microwave synthesis methods[12)]. Based on these several methods, in this study, the solid-state method was chosen because the control

variables were easy and simple. Carbon from teak sawdust waste for use in $LiFePO_4$/C cathode material has never been studied before. Therefore, a study was conducted on the synthesis of carbon as a cathode material with variations in carbonization temperature and a $LiFePO_4$/C battery performance test.

2. Materials and Methods

2.1 Materials

The following materials were used: teak wood sawdust, $FeSO_4$ (Hunan, China), $H_2C_2O_4$ (Yuanping Changyuan Chemicals, China), H_3PO_4 (Brataco, Indonesia), Li_2CO_3 (Merck, Germany), distilled water, carboxymethyl cellulose (CMC), acetylene black (AB), styrene-butadiene rubber (SBR) (MTI, USA), electrolyte $LiPF_6$ and N_2 gas.

2.2 Methods

2.2.1 Carbon Material Synthesis

The preparation of carbon synthesis was started by washing the teak wood sawdust and drying it at 110°C to evaporate the water content. The samples were ground and then sieved and tested using Thermal Gravimetric Analysis (TGA). Furthermore, the samples were carbonized at temperatures of 350, 450, and 550°C for 80 minutes with a N_2 gas stream. A black powder was obtained and continued in the activation process with a 10% H_3PO_4 solution for 24 hours. The sample results were tested using Scanning Electron Microscopy-Energy Dispersive X-ray (SEM-EDX) to determine the morphology and composition of the elements contained in the sample.

2.2.2 Cathode Material Synthesis

As in Fig. 1, iron oxalate was produced using $FeSO_4$ and $H_2C_2O_4$ as much as 27.8 g and 12.6 g, respectively, which were dissolved in 200 mL of distilled water and heated at 60 ℃. The $H_2C_2O_4$ solution was slowly added to the solution and maintained at 60℃ with stirring for 2 hours. The yellow solution was obtained after becoming homogeneous, then filtered and washed to neutral pH with distilled water until a yellow precipitate was obtained and dried in the oven. Furthermore, the manufacture of LFP/C cathode used 11.53 grams of 85% H_3PO_4, and 3.7 grams of Li_2CO_3 mixed with an overhead stirrer and added methanol little by little. After the slurry was formed, 18 g of FeC_2O_4 was added and stirred for 2 hours until homogeneous, followed by drying in the oven. Then, 5% w/w carbon was mixed with dry LFP. The resulting mixture is then heated in a furnace at a temperature of 700℃ for 10 hours with a N_2 gas stream. The resulting LFP/C product was ground with a mortar and pestle and sieved using a 400 mesh sieve and continued with testing using X-Ray Diffractometer (D2 Phaser Bruker, Germany) to determine the crystal structure, SEM-EDX (JEOL JSM-6510LA, Japan) to investigate particle morphology elemental composition contained in the sample, and Fourier Transform Infrared (FTIR) (Shimadzu FTIR, Japan) to detect functional groups.

2.2.3 Battery Assembly and Testing

The LFP/C cathode sheet was prepared by mixing LFP/C:AB:CMC:SBR 89:5:2:3 in distilled water and coated on both sides of the Al foil (Fig. 2). The coated sheets were dried and assembled into a type 18650 cylindrical cell battery with graphite as the anode. The electrolyte used is $LiPF_6$. The assembled battery was tested using a Neware Battery Analyzer (Neware, China) to determine battery capacity and Electrochemical Impedance Spectroscopy (EIS) (Nuvant System Inc., USA) to determine the LFP/C conductivity.

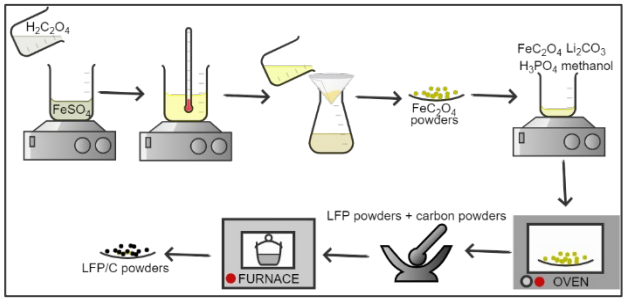

Fig. 1: Experimental method for cathode material synthesis

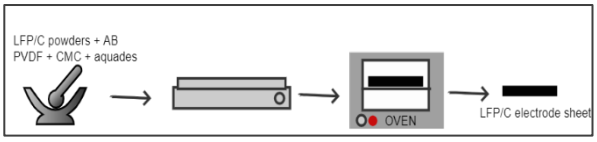

Fig. 2: Experimental method for LFP electrode sheet

3. Results and Discussion

The thermal properties of teak sawdust are depicted in Fig. 3. The temperature range between 30 - 50℃ is the step of removing water content, and the endothermic peak is found on the DTA curve at a temperature of 26.05℃. The decrease in the weight of the two teak sawdust occurred at a temperature of 50 - 370℃. While on the DTA curve, there is a peak at a temperature of around 370℃ due to excessive heat release. This was due to the evaporation of organic matter. The weight also decreases as hemicellulose and cellulose content decompose between 380 - 480℃. Teak sawdust's remaining lignin is believed to be decomposing at temperatures between 480 - 700℃[13]. This is in accordance with Adeleke's research[14], where the thermogravimetric curve of teak sawdust is divided into three different heating stages: first, the drying stage at temperatures below 12℃, the second stage occurs between 125 - 500℃ temperatures when decomposition of hemicellulose, cellulose, and some of the lignin occurs, and the third stage is above the temperature of 500℃ when the decomposition of residual lignin occurs slowly and continuously.

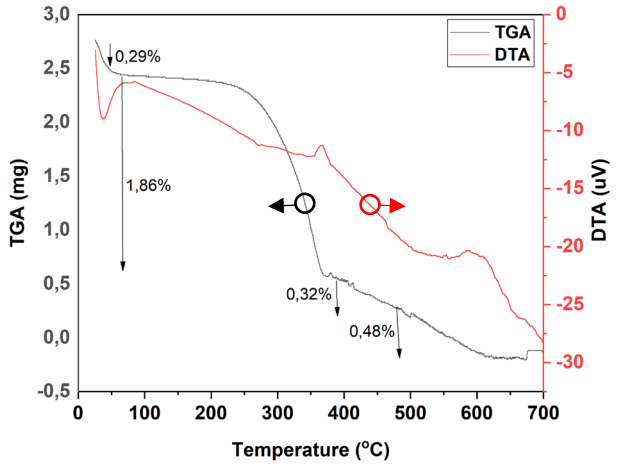

Fig. 3: Results of TGA-DTA teak wood powder

In the carbonization process, it requires impregnation the starting material with a dehydrating chemical agent. H_3PO_4 solution was being used in this research to dehydrate the precursor and extract tar from the biomass material. The chemically treated teak wood biomass in the next step, activation takes place at high temperature in the presence of supporting gases (N_2) that can prevent CO_2 formation and generate pores of diverse sizes in the activated carbon during activation process [14,16].

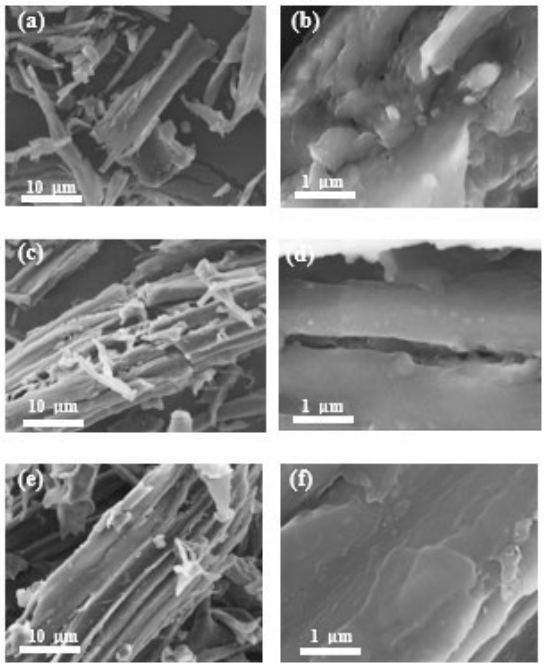

Fig. 4: Surface morphology of carbonized samples C-350: (a) x1000, (b) x10000, (c) x1000, (d) x10000, (e) x1000, and (f) x10000

The higher carbonization temperature, the cells making up the wood become denser and the cell cavities are smaller because increasing the heating temperature will cause a decrease in the moisture content of the wood[15]. This is also shown on how the morphology of samples change significantly (Fig. 4). According to Pavithra's research, teak wood fiber consists of several microfibrils and each fiber has a compact structure[16]. As a result, the SEM image (Fig. 4) reveal that the increasing of the temperature, the more dense and compact the structure of carbon obtains.

Furthermore, from the results of the EDX data, the table of elemental composition contained in the sample can be seen in Table 1. where the carbon element composition of the teak sawdust material is highest in sample C-550, which is 81.73%. This is consistent with Nor's research, which found that the carbonization temperature, followed by the carbonization time, had the greatest impact[17].

Table 1. Elemental composition in carbonized samples

Element	Mass%		
	C-350	C-450	C-550
C	71.55±0.77	78.47±0.86	81.73±0.85
O	28.45±1.37	21.53±1.55	18.27±1.44
Total	100	100	100

These results suggest that the carbon content produced increases with increasing carbonization temperature.

According to JCPDS Card No. 81-1173, it can be seen in Fig. 5 at the tops of the 2θ angle range from 15 - 60°C, indicating that the LFP has an orthorhombic structure[18]. This is by the study of Zhou[19], that sharp and narrow peaks imply a good crystalline phase of the material. Due to the amorphous structure of carbon and its low content in LFP, the carbon peak was not observed and didn't have an impact on the crystal structure[16].

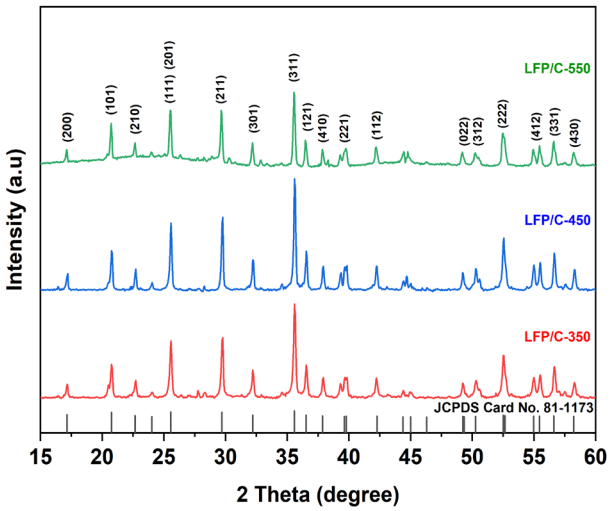

Fig. 5: XRD results of LFP/C

The Debye Scherrer equation was used to determine the crystal size of the LFP/C sample, which is depicted in Table 2. The LFP/C-450 sample had the smallest crystal size, measuring 9.46 nm. This is due to peak broadening, which was discovered at this temperature. Indicating that LFP/C-450 has an amorphous structure contained. High electrochemical performance can be achieved with

smaller crystal sizes by reducing the path length for lithium-ion transport and boosting its diffusion coefficient[21]. This is consistent with Liu's research[22], which found that the phase transition during lithium-ion intercalation and deintercalation can be accelerated by a shorter transport path brought on by a lower crystal size.

Table 2. Crystal size value

Materials	D (nm)
LFP/C-350	12.40
LFP/C-450	9.46
LFP/C-550	12.99

Figure 6 illustrates the particle morphology with and without the addition of carbon, and it reveals that some particles are polyhedral[23]. Without carbon, the LFP material has an average size of particles of 3.68 µm. When compared with LFP/C-350, LFP/C-450, and LFP/C-550 materials which have added carbon material, the average particle sizes are not much different, namely 4.48 µm, 3.73 µm, and 4.52 µm. The smallest particle size is in the LFP/C-450 variation. As a result, the surface area where lithium-ions diffuse during the intercalation and deintercalation processes is greatly increased[23].

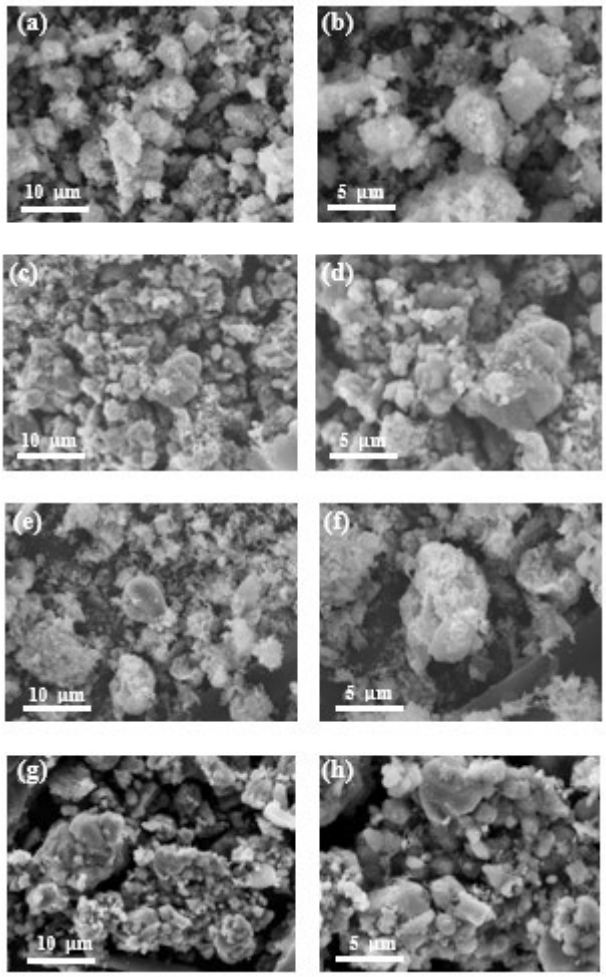

Fig. 6: Surface morphology of samples: (a) LFP without carbon x2500, (b) LFP without carbon x5000, (c) LFP/C-350 x2500, (d) LFP/C-350 x5000, (e) LFP/C-450 x2500, (f) LFP/C-450 x5000, (g) LFP/C-550 x2500, and (h) LFP/C-550 x500

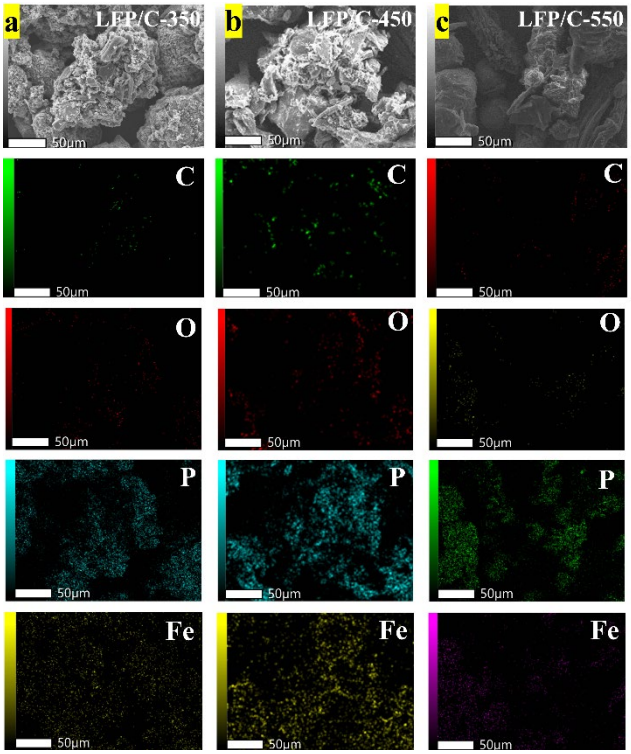

Fig. 7: EDX elemental mapping of the (a) LFP/C-350, (b) LFP/C-450, (c) LFP/C-550.

The EDX test was also conducted to ascertain the chemical elements' composition. Table 3 displays the breakdown of the components found in the sample. Figure 7 shows the mapping results from the EDX test, which can be used to determine the distribution of carbon in the LFP/C-350, LFP/C-450, and LFP/C-550 sample.

Table 3. Elemental composition of LFP/C samples

Element	Mass%		
	LFP/C-350	LFP/C-450	LFP/C-550
C	8.83±0.60	10.06±0.58	51.77±0.80
O	45.09±1.27	43±1.19	27.83±1.16
P	18.33±0.64	13.54±0.55	4.81±0.26
Fe	27.76±1.63	33.41±1.74	15.59±1.01
Total	100	100	100

The FTIR test was used to determine the resulting bond in LFP/C. Figure 8 illustrates that the sample falls between wave numbers 400 – 4000 cm^{-1}. It demonstrates the presence of P-O stretching vibrations at the peaks of waves 1139, 1050, and 956 cm^{-1}. O-P-O stretching vibrations are wave numbers 651, 633, 576, and 549 cm^{-1}. The movement of lithium ions in $LiFePO_4$ is then represented by waves with wavelengths of 499 and 469 cm^{-1} [24].

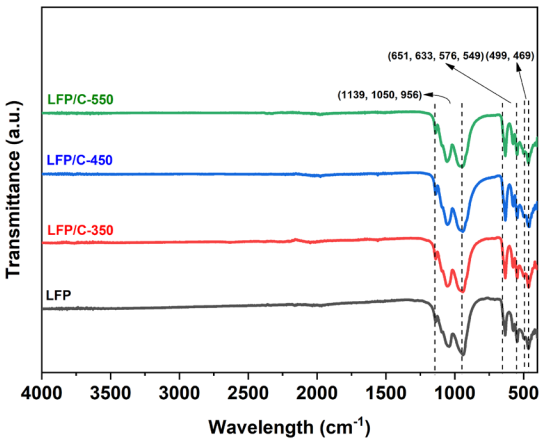

Fig. 8: FTIR results of LFP/C

The three samples almost resemble a semicircle, as shown in Fig. 9. Each diameter's size corresponds to an impedance value, with larger diameters corresponding to higher impedance values and vice versa. This value can affect the conductivity value where the higher the impedance value, the smaller the conductivity value[25]. While the high peak of the semi-circle curve indicates the capacitive nature of the three samples, where the higher the peak of the curve, the lower the capacitive properties it has. The LFP/C-450 sample has the best capacitive properties among the three samples, which are associated with the material's capacity to store Li ions in its structure.

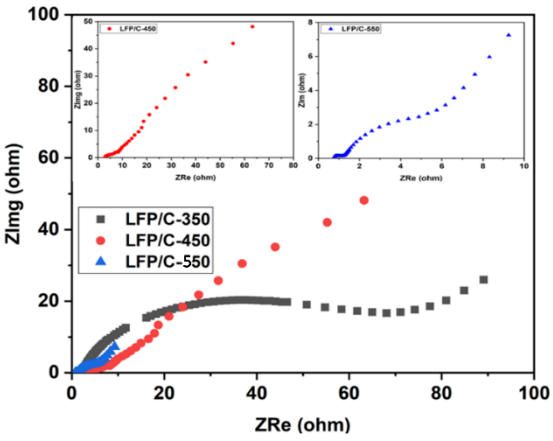

Fig. 9: Nyquist plot of LFP/C

Table 4 shows the result of calculating the value of the cathode conductivity. Based on these results, it is known that the LFP/C-450 sample has the highest conductivity value of 3.31×10^{-3} S/cm. When compared with the LFP material without carbon, which has a conductivity of 10^{-9} S/cm, the sample LFP/C-450 has a higher conductivity value. This also corresponds to the particle size and crystal size of LFP/C-450 which is smaller than the other samples. Additions with different carbon content compositions produce different conductivity values[26,27]. Based on research by Raj & Sil[20], a very high carbon content (too thick a carbon layer) can slow the diffusion of lithium ions so that the rate of charge transfer in the material is restrained.

Table 4. Cathode conductivity values

Materials	Conductivity (S/cm)
LFP/C-350	0.23×10^{-3}
LFP/C-450	3.31×10^{-3}
LFP/C-550	1.82×10^{-3}

Figure 10 illustrates the charge-discharge formation curve of an LFP/C battery with graphite as the anode and a current rate of 0.03C applied to the battery during the electrochemical performance test. The curve with increasing voltage shows the charging process in which the lithium at the cathode is transferred to the anode through the electrolyte medium. While the voltage drop curve depicts the process by which lithium moves from the anode to the cathode during a discharge. Table 5 shows the results of the specific charge-discharge capacity, initial coulombic efficiency, and energy density of the three samples. The highest specific capacity was in the LFP/C-450 sample, which was 36.18 mAh/g. This could be since the average particle size and crystal size in the LFP/C-450 sample were smaller than the other samples, thereby shortening the Li+ ion diffusion path and expanding the specific contact area between particles which could increase charge transfer during intercalation and deintercalation[28]. However, the specific capacity results are still far from commercial $LiFePO_4$ battery which has a capacity of 170 mAh/g. This could be due to the different test methods where in this study the full-cell method was carried out while the theoretical capacity of commercial $LiFePO_4$ batteries was carried out using the half-cell method. In addition, the sample material is exposed to air for too long when filtering LFP/C solids which can cause damage to the sample[23]. Kashi reported a specific discharge capacity at the formation of 86 mAh/g with an initial coulomb efficiency of 78%[29].

In this study, the coulombic efficiency during formation was 38.08%, 31.73%, and 27.6%. This could be attributed to the non-uniform charge allocation formed at the electrode/electrolyte interface resulting in uncontrolled Li deposition, resulting in Li dendrites which could pose a safety hazard. During the charge/discharge process, the Li metal anode's solid electrolyte interface (SEI) can continually form and break. The SEI is unstable, leading to low coulombic efficiency, as a result of the battery's recurrent usage of Li and electrolyte supplies [30-33]. On the other hand, during the charge/discharge process, the Li metal anode's solid electrolyte interface (SEI) can continually break and form. Low coulombic efficiency is caused by the SEI being unstable as a result of the battery's frequent utilization of Li and electrolyte supplies[34,35].

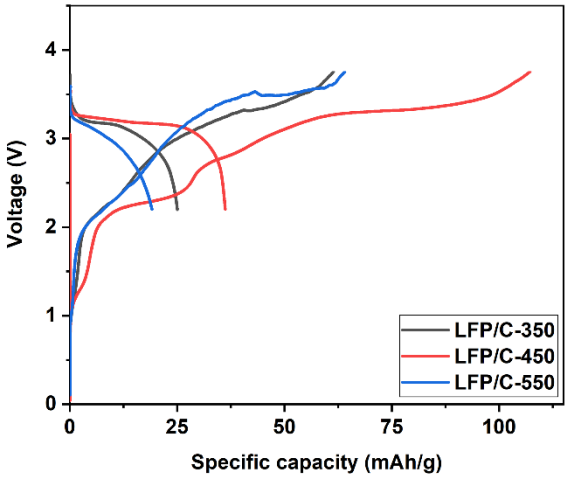

Fig. 10: Specific capacity results of LFP/C battery

Table 5. Calculation results of the charge-discharge test

Materials	Specific Charge Capacity (mAh/g)	Specific Discharge Capacity (mAh/g)	Initial Coulombic Efficiency (%)	Specific Discharge Energy (mWh/g)
LFP/C-350	65.7	25.02	38.08	55.03
LFP/C-450	114	36.18	31.73	79.59
LFP/C-550	69.32	19.13	27.6	42.08

4. Conclusion

Carbon was successfully synthesized from teak sawdust using the carbonization method and the activation process from phosphoric acid. Variations in carbonization temperature affect the composition of carbon content in each sample. This was confirmed in the SEM-EDX test where the highest carbon content was obtained at a carbonization temperature of 550 ℃ at 81.73%. The addition of carbon to the LFP cathode material can increase the conductivity value of the material where the highest conductivity is shown in the LFP/C-450 sample of 3.31×10^{-3} S/cm. This result is higher than the commercial LFP of 10^{-9} S/cm. Meanwhile, the highest specific battery capacity of the three samples is the LFP/C-450 sample of 36.18 mAh/g. This has been confirmed on specific capacity tests and EIS tests supported by XRD, SEM-EDX, and FTIR test results. In this case, the use of carbon from teak sawdust can increase the conductivity of the LFP, influencing lithium-ion transport during intercalation/deintercalation. However, there are still weaknesses in the form of low specific capacity results due to different test methods and samples being exposed to air for an excessive period.

Acknowledgements

This paper was facilitated by the Centre of Excellence for Electrical Energy Storage Technology, Sebelas Maret University, Surakarta, Indonesia.

References

1) Q. Wang, B. Mao, SI. Stoliarov, and J. Sun, "A review of lithium-ion battery failure mechanisms and fire prevention strategies," *Progress in Energy and Combustion Science.*, **73** 95-131 (2019). doi:10.1016/j.pecs.2019.03.002.
2) S. Ma, M. Jiang, P. Tao, C. Song, J. Wu, J. Wang, T. Deng, and W. Shang, "Temperature effect and thermal impact in lithium-ion batteries: A review," *Progress in Natural Science: Materials International.*, **28** (6) 653-666 (2018). doi:10.1016/j.pnsc.2018.11.002.
3) B. Priyono, B. Rifky, F. Zahara, and A. Subhan, "Enhancing Performance of $Li_4Ti_5O_{12}$ with Addition of Activated Carbon from Recycled PET Waste as Anode Battery Additives," *Evergreen*. **9**(2) 563-570 (2022). doi:10.5109/4794188.
4) H. Widiyandari, O.A. Putra, R. Suryana, and I. Firdaus, "Highly Porous and Thermally Stable Poly (vinylidene fluoride) Separators: Effects of Solvent and Colloidal SiO_2 Concentration," *Evergreen.* **9**(2) 443-450 (2022). doi:10.5109/4794170.
5) H. Widiyandari, A.N. Sukmawati, H. Sutanto, C. Yudha, and A. Purwanto, "Synthesis of $LiNi_{0.8}Mn_{0.1}Co_{0.1}O_2$ cathode material by hydrothermal method for high energy density lithium-ion battery," *In Journal of Physics: Conference Series.*, **1153** (1) 012074 (2019). doi:10.1088/1742-6596/1153/1/012074/meta.
6) D. Ren, Y. Shen, Y. Yang, L. Shen, B.D.A. Levin, Y. Yu, D.A. Muller, and H.D. Abruna, "Systematic optimization of battery materials: key parameter optimization for the scalable synthesis of uniform, high-energy, and high stability LiNi0.6Mn0.2Co0.2O2 cathode material for lithium-ion batteries," *ACS applied materials & interfaces*., **9** (41) 35811-35819 (2017). doi:10.1021/acsami.7b10155.
7) Y. Yang, X. Meng, H. Cao, X. Lin, C. Liu, Y. Sun, Y. Zhang, and Z. Sun, "Selective recovery of lithium from spent lithium iron phosphate batteries: a sustainable process." *Green chemistry.*, **20** (13) 3121-3133 (2018). doi:10.1039/C7GC03376A.
8) L. Chen, W. Feng, Z. Pu, X. Wang, W. Su, M. Li, C. Song, Z. Shi, and Y. Zheng, "Effects of Citric Acid on the Preparation of a $LiFePO_4$@C Cathode Material Assisted by Biomineralization," *Int. J. Electrochem. Sci.,* **14** 8048-8057 (2019). doi: 10.20964/2019.08.78.
9) Y. Wibisono, A. Amanah, A. Sukoyo, and F. Anugroho, "Activated carbon loaded mixed matrix membranes extracted from oil palm empty fruit bunches for vehicle exhaust gas adsorbers,"

Evergreen. **8**(3) 593-600 (2021). doi:10.5109/4491651.

10) E. Erawati, and E.F.N. Afifah, "Pembuatan Karbon Aktif dari Gergaji Kayu Jati (Tectona Grandis L, F)(Ukuran Partikel dan Jenis Aktivator)," *Proceeding of The URECOL.*, 97-104 (2019). http://repository.urecol.org/index.php/proceeding/article/view/487.
11) N.A.B. Othman, T. Kim, A. Imamura, J. Miyawaki, I. Mochida, and S.H. Yoon, "Investigation on H_2S Removal Factors of Activated Carbons Derived from Waste Palm Trunk," *Evergreen.* **7** 7-11 (2013). http://ncrs.cm.kyushu-u.ac.jp/ncrs2/index.html.
12) G. Hu, X. Xie, Y. Cao, L. Xu, K. Du, W. Wang, and Z. Peng, "Ultrasonic-assisted synthesis of $LiFePO_4$/C composite for lithium-ion batteries using iron powder as the reactant," *Journal of Alloys and Compounds.*, **773** 1165-1171 (2019). doi:10.1016/j.jallcom.2018.09.270.
13) J.B. Mathangi, M.S. Sharma, B.M. Jacquline, and M.H. Kalavathy, "Development of carbon-based material from biomass for the removal of Ni^{2+} and CO_2 from fluid phase," *Vacuum*., **158** 236-248 (2018). doi:10.1016/j.vacuum.2018.09.056.
14) A. Adeleke, P. Ikubanni, J. Odusote, T. Orhadahwe, O. Lasode, S. Adegoke, and O. Adesina, "Evaluation of Non-Isothermal Kinetic Parameters for Pyrolysis of Teak Wood using Model-Fitting Techniques," *Trends in Sciences.*, **18** (24) 1432-1432 (2021). doi:10.48048/tis.2021.1432.
15) S. Huang, L. Wang, Y. Li, C. Liang, & J. Zhang. "Novel Ti3C2T x MXene/epoxy intumescent fire‐retardant coatings for ancient wooden architectures." *Journal of Applied Polymer Science*, **138** (27), 50649 (2021). doi:10.1002/app.50649.
16) R. Pavithra, S. Gunasekaran, E. Sailatha, and S. Kamatachi, "Isolation and Characterization of Cellulosic Nano Fibrils from Teak Wood," *Journal of Applied Science and Engineering Methodologie.s*, **2** (2) 246-249 (2016). http://www.jasem.in/2016/V2SI2246249.
17) N.M. Nor, L.C Lau, K. Teong, and A.R. Mohamed, "Synthesis of activated carbon from lignocellulosic biomass and its applications in air pollution control—a review," *Journal of Environmental Chemical Engineering.*, **1** (4) 658-666 (2013). doi:10.1016/j.jece.2013.09.017.
18) J. Xia, F. Zhu, G. Wang, L. Wang, Y. Meng, and Y. Zhang, "Synthesis of $LiFePO_4$/C using ionic liquid as carbon source for lithium-ion batteries," *Solid State Ionics.*, **308** 133-138 (2017). doi:10.1016/j.ssi.2017.06.007.
19) N. Zhao, Y. Li, X. Zhao, X. Zhi, and G. Liang, "Effect of particle size and purity on the low temperature electrochemical performance of $LiFePO_4$/C cathode material," *Journal of Alloys and Compounds.*, **683** 123-132 (2016). doi:10.1016/j.jallcom.2016.04.070.
20) H. Raj and A. Sil, "Effect of carbon coating on electrochemical performance of $LiFePO_4$ cathode material for Li-ion battery," *Ionics.*, **24** (9) 2543-2553 (2018). doi:10.1007/s11581-017-2423-0.
21) Y. Liu, J. Gu, J. Zhang, J. Wang, N. Nie, Y. Fu, W. Li, and F. Yu, "Controllable synthesis of nano-sized $LiFePO_4$/C via a high shear mixer facilitated hydrothermal method for high-rate Li-ion batteries," *Electrochimica Acta.*, **173** 448-457 (2015). doi:10.1016/j.electacta.2015.05.103.
22) Y. Liu, D. Liu, Q. Zhang, D. Yu, J. Liu, and G. Cao, "Lithium iron phosphate/carbon nanocomposite film cathodes for high energy lithium-ion batteries," *Electrochimica Acta.*, **56** (5) 2559-2565 (2011). doi:10.1016/j.electacta.2010.11.050.
23) M, Arinawati, A.P. Hutama, C.S. Yudha, M, Rahmawati, and A. Purwanto, "Facile rheological route method for $LiFePO_4$/C cathode material production," *Open Engineering.*, **11** (1) 669-676 (2021). doi:10.1515/eng-2021-0068.
24) W. Li, J. Hwang, W. Chang, H. Setiadi, K.Y. Chung, and J. Kim, "Ultrathin and uniform carbon-layer-coated hierarchically porous $LiFePO_4$ microspheres and their electrochemical performance," *The Journal of Supercritical Fluid.*, **116** 164-171 (2016). doi:10.1016/j.supflu.2016.05.007.
25) B. Priyono, B. Rifky, F. Zahara, & A. Subhan. "Enhancing Performance of $Li_4Ti_5O_{12}$ with Addition of Activated Carbon from Recycled PET Waste as Anode Battery Additives." *Evergreen.* **9**(2), 563-570 (2022). doi: https://doi.org/10.5109/4794188.
26) K. L. A. Cao, A. M. Rahmatika, Y. Kitamoto, M. T. T. Nguyen, & T. Ogi. "Controllable synthesis of spherical carbon particles transition from dense to hollow structure derived from Kraft lignin.' *Journal of Colloid and Interface Science*, 589, 252-263 (2021). doi: https://doi.org/10.1016/j.jcis.2020.12.077
27) N. Grioui, K. Halouani, A. Zoulalian, & F. Halouani. "Thermogravimetric analysis and kinetics modeling of isothermal carbonization of olive wood in inert atmosphere." *Thermochimica Acta*, 440(1), 23-30 (2006). doi: https://doi.org/10.1016/j.tca.2005.09.018
28) Z. Nannan, L. Yongsheng, Z. Xiaoke, W. Li, Z. Xinxin, W. Yamian, & G. Liang. "Effect of Ce^{3+} doping on the properties of $LiFePO_4$ cathode material." *Journal of Rare Earths*, **34** (2), 174-180 (2016). doi: https://doi.org/10.1016/S1002-0721(16)60011-X.
29) R. Kashi, M. Khosravi, and M. Mollazadeh, "Effect of carbon precursor on electrochemical performance of $LiFePO_4$-C nano composite synthesized by ultrasonic spray pyrolysis as cathode active material for Li ion battery," *Materials Chemistry and Physics*., **203** 319-332 (2018). doi:10.1016/j.matchemphys.2017.10.021.
30) T. Zhou, J. Shen, Z. Wang, J. Liu, R. Hu, L. Ouyang, Y. Feng, H. Liu, Y. Yu, and M. Zhu, "Regulating lithium nucleation and deposition via MOF‐derived Co@C‐modified carbon cloth for stable Li metal

anode," *Advanced Functional Material*., **30** (14) 1909159 (2020). doi:10.1002/adfm.201909159.
31) U. Meda, L. Lal, M. Sushantha, & P. Garg. Solid Electrolyte Interphase (SEI), a boon or a bane for lithium batteries: A review on the recent advances. *Journal of Energy Storage*, 47, 103564, (2022). Doi: https://doi.org/10.1016/j.est.2021.103564
32) H. Wang, D. Zhai, & F. Kang. Solid electrolyte interphase (SEI) in potassium ion batteries. *Energy & Environmental Science*, *13*(12), 4583-4608, (2020). Doi: https://doi.org/10.1039/D0EE01638A
33) M. Nizam, & M. R. A. Putra. Heat Management on LiFePo4 Battery Pack for Eddy Current Brake Energy Storage on Rapid Braking Processes. *Evergreen. 9*(2), 451-456, (2022). Doi: https://doi.org/10.5109/4794171
34) R. N. Anisa, S. Y. Cornelius, R. Mintarsih, S. N. Shofirul, J. Arif, H. Widiyandari, & A. Purwanto. Structural and Electrochemical Analysis of Iron Doping in LiNi_0. 6-x Mn_0. 2 Co_0. 2 Fe_x O_2 battery. *Evergreen*, 8(1), 82-88. (2021). Doi: 10.5109/4372263
35) H. Adenusi, G. A. Chass, S. Passerini, K. V. Tian, & G. Chen. Lithium batteries and the solid electrolyte interphase (SEI)—progress and outlook. *Advanced Energy Materials*, 13(10), 2203307, (2023). Doi: https://doi.org/10.1002/aenm.202203307